Journal of Alloys and Compounds 503 (2010) 19–24

Contents lists available at ScienceDirect

Journal of Alloys and Compounds

journal homepage: www.elsevier.com/locate/jallcom

Corrosion and pitting behaviour of ultrafine eutectic Ti–Fe–Sn alloys

R. Sueptitz[a,*], J. Das[b], S. Baunack[a], A. Gebert[a], L. Schultz[a,c], J. Eckert[a,c]

[a] IFW Dresden, P.O. Box 27 01 16, D-01171 Dresden, Germany
[b] Department of Metallurgical and Materials Engineering, Indian Institute of Technology, Kharagpur 721 302, West Bengal, India
[c] Dresden University of Technology, Institute of Materials Science, D-01062 Dresden, Germany

ARTICLE INFO

Article history:
Received 8 March 2010
Received in revised form 3 May 2010
Accepted 5 May 2010
Available online 24 May 2010

Keywords:
Metals and alloys
Rapid-solidification
Corrosion
Microstructure

ABSTRACT

Ultrafine structured $Ti_{70.5}Fe_{29.5}$ and $Ti_{67.79}Fe_{28.36}Sn_{3.85}$ eutectic rods comprising of β-Ti and TiFe phases were prepared by copper mould casting. The corrosion and passivation behaviour were investigated in halide free aqueous media (pH 1–13) by means of potentiodynamic polarisation and potentiostatic current transient measurements. Both eutectic alloys exhibit excellent corrosion resistance due to spontaneous passivation. The passive film compositions grown several nanometres on single phase polycrystalline specimens were analyzed with Auger electron spectroscopy. They consist of oxidized Ti and Fe species. Layers grown in strongly acidic environment are depleted in Fe. Sn was detected only on layers grown on the constituent β-Ti phase and only in the metallic state. The pitting susceptibility was investigated in strongly acidic media (pH ≤ 1) containing 0.1–3 M of chloride ions. The Sn-containing eutectic alloy was found to be more susceptible to pitting corrosion.

1. Introduction

Usually mechanical properties of alloys can be improved by refining their microstructure. The strength of crystalline alloys obeys the Hall–Petch relation [1,2] which predicts an increase of the hardness with decreasing grain size down to about 10 nm. However, fine-grain crystalline alloys generally exhibit low ductility and limited work hardening behaviour [3]. Ti-alloys with low density, high strength and ductility and high chemical stability are of strong interest for energy efficient construction. It has been reported that the ductility of nanocrystalline materials can be enhanced by embedding a micrometer-sized soft phase in a nano-structured matrix [4–7]. Louzguine et al. [4] have reported the formation of a composite which contains micron-sized supersaturated β-Ti solid solution embedded in a fine-structured β-Ti/TiFe eutectic in $Ti_{65}Fe_{35}$. The composite exhibits a compressive strength of 2200 MPa and compressive strain to fracture of 6.7%. Das et al. [8] reported the eutectic $Ti_{70.5}Fe_{29.5}$ alloy to exhibit a maximum strength of 1935 MPa and strain to failure of 2.6%. Upon addition of Sn to $Ti_{70.5}Fe_{29.5}$ the fine-structured β-Ti/TiFe eutectic composite $Ti_{67.79}Fe_{28.36}Sn_{3.85}$ with a lamellar spacing of about 300 nm exhibits compressive strength of 2260 MPa with compressive strain to failure of 9.6%.

With respect to the corrosion behaviour, a nano-sized grain structure can lead to poor performance. The effect of galvanic coupling between the finely distributed phases can be promoted and the high density of surface heterogeneities can support the local dissolution or passive layer breakdown [9]. On the other hand, a large fraction of grain boundaries may support the diffusion of constituent atoms to the surface and thus, can lead to an accelerated and more uniform passive layer growth [10–12].

Due to the high content of Ti, the alloy $Ti_{67.79}Fe_{28.36}Sn_{3.85}$ is expected to show in principle spontaneous passivity and a high resistance against corrosion in a wide pH value range. However, the significant fraction of Fe in ultrafine distribution in the lamellar microstructure might affect the passivation ability in particular in acidic media and also the resistance against pitting corrosion. The aim of the present study is to investigate the corrosion behaviour of the ultrafine $Ti_{67.79}Fe_{28.36}Sn_{3.85}$ and $Ti_{70.5}Fe_{29.5}$ eutectics in different aqueous media. The role of the ultrafine microstructure and of their single constituent phases as well as the elements on the passivation ability and pitting susceptibility are analyzed. This will allow the evaluation of the potential of the alloys for possible application under severe environmental conditions.

2. Experimental

Ingots of the $Ti_{70.5}Fe_{29.5}$ and $Ti_{67.79}Fe_{28.36}Sn_{3.85}$ eutectics as well as their constituent single phases, i.e. the β-Ti solid solutions ($Ti_{80}Fe_{20}$ and $Ti_{82.3}Fe_{9.2}Sn_{8.5}$) and the TiFe intermetallic phases ($Ti_{51}Fe_{49}$ and $Ti_{52.5}Fe_{46.8}Sn_{0.7}$), were prepared in an electrical arc furnace under Ar atmosphere from the elements with a purity of 99.99%. The ingots were re-melted and cast into copper moulds under Ar atmosphere in a Hukin-type cold-crucible levitation facility in order to obtain rods of 6 mm diameter and of 80 mm length.

Cylindrical samples of 15 mm length were electrically contacted and embedded in epoxy resin for microstructural observation using scanning electron microscopy

* Corresponding author. Tel.: +49 351 4659 715; fax: +49 351 4659 540.
E-mail address: r.sueptitz@ifw-dresden.de (R. Sueptitz).

0925-8388/$ – see front matter © 2010 Elsevier B.V. All rights reserved.
doi:10.1016/j.jallcom.2010.05.052

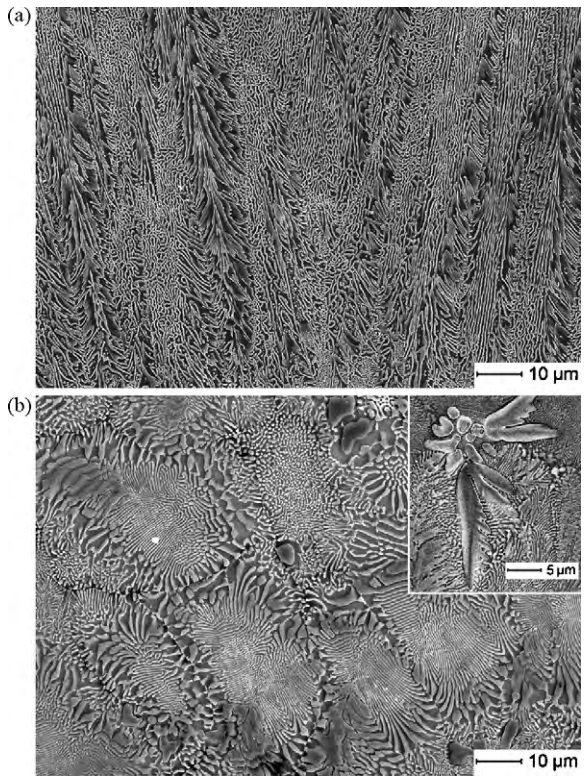

Fig. 1. (a) SEM image of $Ti_{70.5}Fe_{29.5}$ eutectic, bright contrast: TiFe intermetallic phase, dark contrast: β-Ti solid solution (etched in HNO_3/HF solution) and (b) SEM image of $Ti_{67.79}Fe_{28.36}Sn_{3.85}$ eutectic, bright contrast: TiFeSn intermetallic phase, dark contrast: β-Ti solid solution; inset: Sn-rich phase $Ti_{81}Sn_{19}$ (etched in HNO_3/HF solution).

(SEM) (Jeol JSM 6400) and for electrochemical measurements. The phase analysis of each cast sample was conducted by X-ray diffraction (Philips 'PW 1830', Co-K_α radiation). Samples of Fe and Ti (99.8% purity) were prepared for comparative investigations. For electrochemical testing, the embedded samples were grounded with emery paper down to grit 4000 and further polished with 1 μm diamond suspension. All electrochemical experiments were performed in a three-electrode cell using a Pt net as counter electrode and a saturated calomel reference electrode (SCE) (E = 241 mV vs. SHE). The electrolyte solutions, 0.1 M H_2SO_4 (pH 1), 0.5 M phthalate buffer (pH 5), 0.3 M borate buffer (pH 8.4) and 0.1 M NaOH (pH 13), were purged with nitrogen for 1 h before each experiment. For potential control a 'Solartron SI 1287 Electrochemical Interface' was used. After monitoring the open circuit potential (OCP) for 1 h, potentiodynamic polarisation measurements were performed with a scan rate of 0.5 mV/s. The potential was scanned from −100 mV vs. OCP to 2000 mV vs. SCE.

The oxide layers were investigated using Auger electron spectroscopy (AES) depth profiling ('Auger Microprobe PHI 600'). Depth profiling was performed by in situ sputtering with Ar ions of 1.5 keV with an equivalent sputtering rate in TiO_2 of 1.4 nm/min.

The pitting susceptibility was analyzed with potentiodynamic polarisation measurements in 0.1 M H_2SO_4 containing different amounts of KCl and in 1 M and 3 M HCl solutions. Pit morphologies were characterized using SEM. All the electrochemical experiments were repeated at least three times in order to reveal the reproducibility of the data.

3. Results and discussion

3.1. Microstructure

SEM images of the microstructure of the as-cast $Ti_{70.5}Fe_{29.5}$ and $Ti_{67.79}Fe_{28.36}Sn_{3.85}$ eutectic are shown in Fig. 1(a) and (b), respectively. The size of the eutectic colonies is estimated to vary between (20 ± 10) μm width × (75 ± 25) μm length with weakly pronounced colony boundaries in $Ti_{70.5}Fe_{29.5}$. The lamellar spacing was found to be ∼500 nm. However, oval-shaped eutectic colonies of 20–50 μm size with pronounced colony boundaries have been observed in the case of $Ti_{67.79}Fe_{28.36}Sn_{3.85}$ as shown in Fig. 1(b). In the centre of these colonies the eutectic spacing is about 300 nm and becomes broader towards the boundaries, where the TiFe phase appears partially in globular shape embedded in β-Ti. A more detailed description of the microstructure formation is reported in the literature [8,13,14]. However, an additional dendritic-shaped phase was found in the boundary regions of the eutectic colonies at the centre region of the $Ti_{67.79}Fe_{28.36}Sn_{3.85}$ rods, i.e. where the lowest cooling rate was achieved as shown in the inset of Fig. 1(b). XRD investigations (not shown here) displayed the reflections of the TiFe intermetallic and β-Ti solid solution phases only. Thus, the volume fraction of this unknown phase is small and should be less then 5 vol.%. Its composition was determined by AES to be $Ti_{81}Sn_{19}$ without any trace of Fe. Therefore, according to the Ti–Sn phase diagram [15] it is expected the phase to be the hexagonal Ti_3Sn intermetallic phase [16].

Further microstructural analysis was performed for the constituent single phases of the eutectic alloys. The single phase polycrystalline β-Ti specimens ($Ti_{80}Fe_{20}$ and $Ti_{82.3}Fe_{9.2}Sn_{8.5}$) solidified into dendrites with an average size of about 50 μm. However, the Sn-containing phase exhibits much larger dendrites of up to 200 μm including small pores. The single phase polycrystalline TiFe intermetallic specimens ($Ti_{51}Fe_{49}$ and $Ti_{52.5}Fe_{46.8}Sn_{0.7}$) show dendritic microstructure with average cell size of 100 μm. In the case of the TiFe phase without Sn the directed solidification from the rim towards the centre of the sample is more pronounced and some cracks formed between the dendrites.

3.2. General corrosion and anodic passivation behaviour

In order to analyze the anodic behaviour of the eutectic alloys and their constituent single phases in electrolytes with different pH values, potentiodynamic polarisation studies were performed. Fig. 2 depicts values of the corrosion potentials, the corrosion current densities and the passive current densities which were determined from the recorded polarisation curves. The comparison of the data obtained in H_2SO_4 and in NaOH solution reveals a shift of the corrosion potential towards more negative values with increasing pH value. This corresponds to the shift of the hydrogen reduction potential with increasing pH. The corrosion potential is remarkable anodic in the borate buffer solution and depends strongly on the sample composition in the phthalate buffer solution. As origin of this behaviour we expect a specific adsorption of the anions of the buffer solutions. The corrosion current densities are low in general but an enhanced reactivity of the intermetallic TiFe phases is observed in acidic environment. Furthermore, the $Ti_{70.5}Fe_{29.5}$ exhibits a higher corrosion rate than $Ti_{67.79}Fe_{28.36}Sn_{3.85}$ in strongly acidic media. The passive current densities are also low in general, especially in weakly acidic and weakly basic media suggesting a highly protective effect of the passive layers.

Due to the similar behaviour of the alloys in strongly and weakly acidic solutions, and in strongly and weakly basic solutions, respectively, only the polarisation curves recorded in strongly acidic and strongly basic environment will be further discussed in detail. Fig. 3 shows potentiodynamic polarisation curves of both eutectic alloys and their main constituent elements Fe and Ti recorded in 0.1 M H_2SO_4 (pH 1). Additionally, in Fig. 4 potentiodynamic polarisation curves of $Ti_{67.79}Fe_{28.36}Sn_{3.85}$ and its constituent single phases are shown, and as an inset, curves of $Ti_{70.5}Fe_{29.5}$ and its constituent single phases for a potential region close to their free corrosion potential.

Pure Fe dissolves actively at its corrosion potential and during anodic polarisation until the passivation potential of ∼0.25 V vs. SCE is reached, where the current density is reduced drastically. Upon further polarisation the passive current density remains nearly constant until the onset of oxygen evolution (transpassivity). In contrast, pure Ti as typical valve metal passivates spontaneously

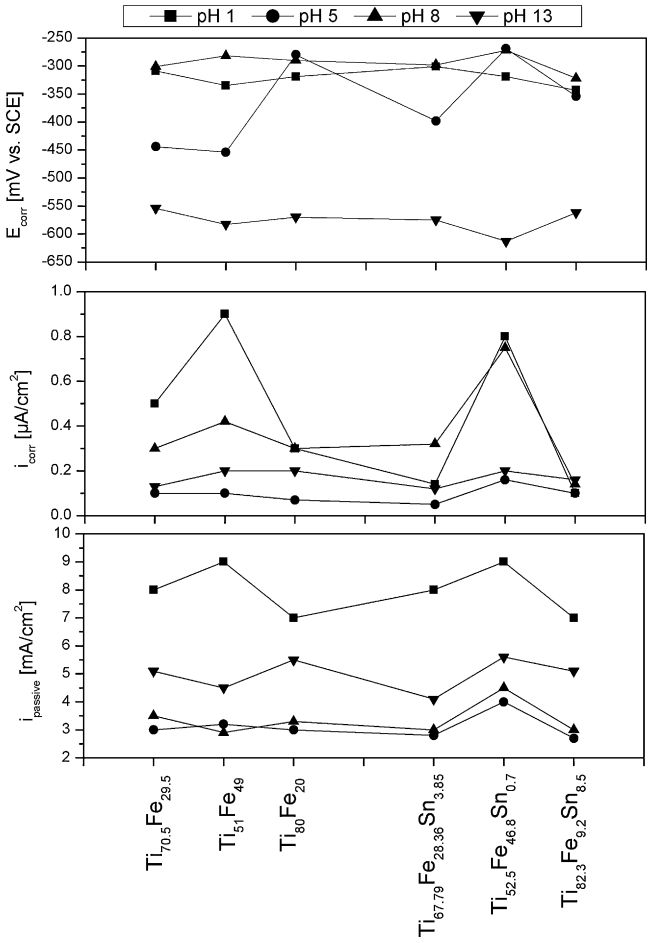

Fig. 2. Corrosion potentials E_{corr}, corrosion current densities i_{corr} and passive current densities $i_{passive}$ of the eutectic alloys and their constituent single phase polycrystalline specimens determined in electrolytes of pH 1–13.

and therefore, exhibits a comparatively low free corrosion current density. However, during anodic polarisation the current density rises gradually with a characteristic step at ~1 V vs. SCE [17]. Similar to Ti, both eutectic alloys and their constituent single phases exhibit spontaneous passivity. Their corrosion potentials lie in between the corrosion potential values of Ti and Fe which may be indicative for the formation of a mixed oxide-type passive layer. However,

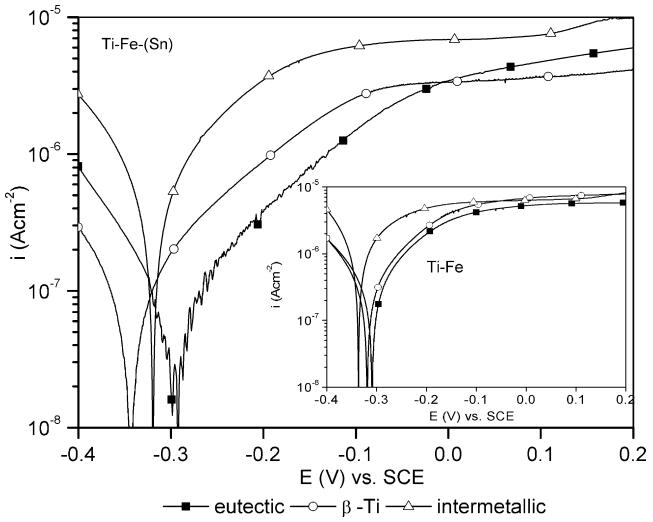

Fig. 4. Current density–potential curves of the eutectic alloys and their single phase specimens recorded in 0.1 M H_2SO_4 (scan rate of 0.5 mV/s) for $Ti_{67.79}Fe_{28.36}Sn_{3.85}$; inset: $Ti_{70.5}Fe_{29.5}$.

considering the active behaviour of pure Fe at the free corrosion potentials of the alloys, a partial dissolution of Fe leading to an enrichment of Ti species in the oxide layer appears to be reasonable. However, it is obvious in Figs. 2 and 4, that due to their high Fe fraction the intermetallic phases ($Ti_{51}Fe_{49}$ and $Ti_{52.5}Fe_{46.8}Sn_{0.7}$) exhibit increased corrosion current densities compared to the β-Ti solid solutions and the eutectic alloys, which behave Ti-like at low polarisation. Moreover, $Ti_{67.79}Fe_{28.36}Sn_{3.85}$ shows a lower corrosion current density than $Ti_{70.5}Fe_{29.5}$. Similar effect of the Sn addition can also be seen in the case of single phase β-Ti specimens. $Ti_{82.3}Fe_{9.2}Sn_{8.5}$ exhibits a lower free corrosion current density than $Ti_{80}Fe_{20}$.

At higher potentials in the passive range, i.e. potentials ≥0.5 V vs. SCE until the onset of transpassivity, both eutectic alloys behave Fe-like. They establish passive current densities that are independent of the applied potential, as shown in Fig. 3. However, in the transpassive region the current densities for both eutectic alloys are in between the values of pure Ti and Fe.

In Fig. 5 anodic polarisation curves of the eutectic alloys and their constituent elements Fe and Ti in 0.1 M NaOH solution (pH 13) are shown. In this environment both eutectic alloys, their constituent phases (not shown) and the main constituent elements Ti

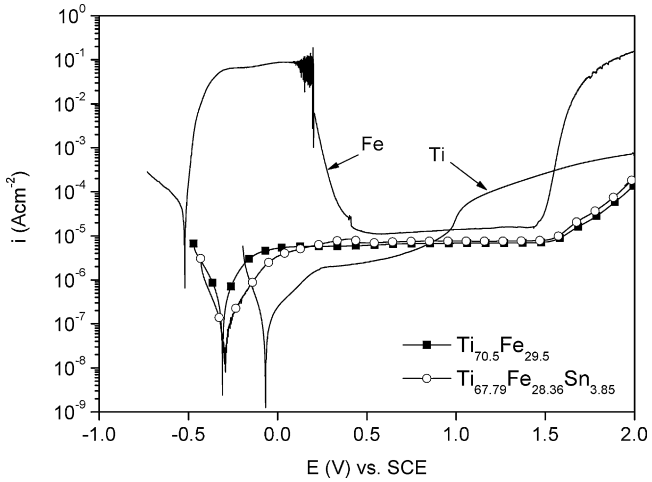

Fig. 3. Current density–potential curves of the eutectic alloys and the constituent elements Fe and Ti recorded in 0.1 M H_2SO_4 (scan rate of 0.5 mV/s).

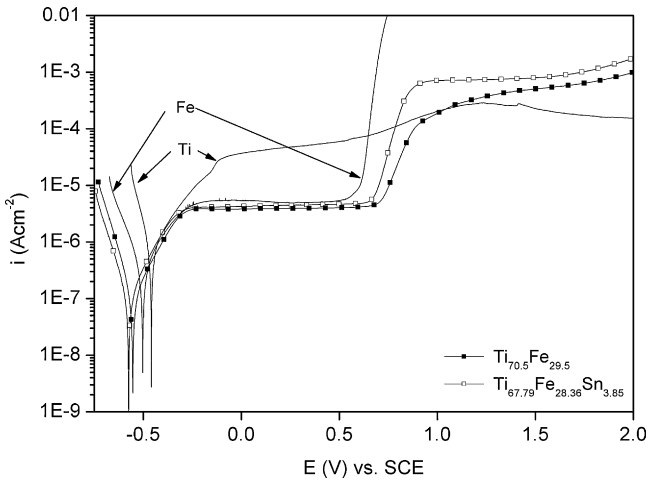

Fig. 5. Current density–potential curves of the eutectic alloys and the constituent elements Fe and Ti recorded in 0.1 M NaOH (scan rate of 0.5 mV/s).

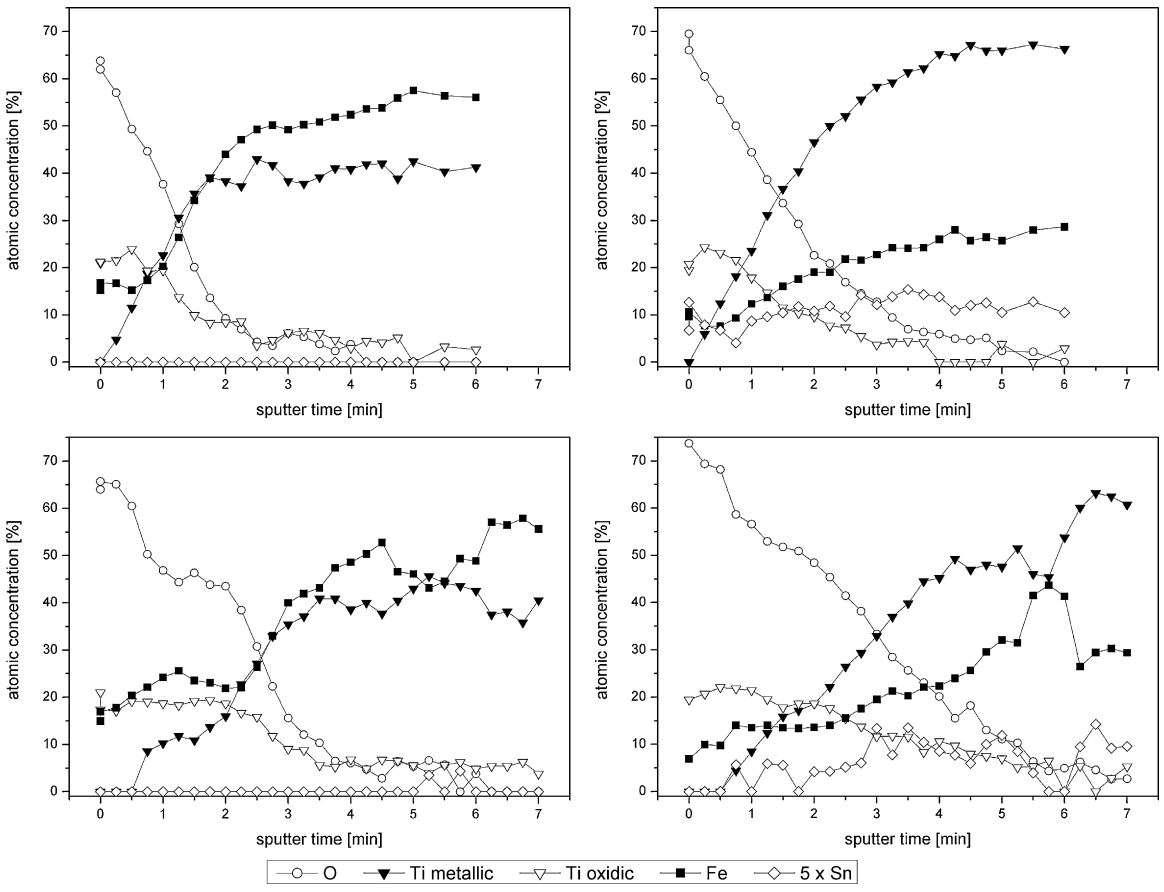

Fig. 6. Chemical depth profiles (AES) of surfaces of the ternary TiFeSn intermetallic phase (left) and the ternary β-Ti solid solution (right) passivated for 60 min at 500 mV vs. SCE in 0.1 M H_2SO_4 (top) and 0.1 M NaOH (bottom).

and Fe exhibit spontaneous passivity. It should be noted that all corrosion potentials of the alloyed species (−0.61 to −0.55 V vs. SCE) adjust at slightly more negative potentials than those for the pure elements Fe (−0.46 V vs. SCE) and Ti (−0.5 V vs. SCE). The eutectic alloys as well as their constituent single phase specimens behave like Fe Near the free corrosion potential regarding the Tafel slopes, but exhibit a lower free corrosion current density than the pure elements. In addition, the corrosion current densities of both eutectic alloys are lower than those of their constituent single phases. Therefore, it is expected that strong barrier-type passive films with different compositions must grow rapidly on each phase of the ultrafine structured alloys. In the passive range the behaviour of the alloys is Fe-like showing a passive current density that is nearly independent on the potential until the onset of transpassivity. The slope of the potentiodynamic polarisation curves of the eutectic alloys is slightly lower than for pure Fe at the initial potential range of transpassivity (∼0.6–0.9 V vs. SCE), but decreases drastically at a potential of about 0.9 V vs. SCE. However, at more positive potential in the transpassive region the eutectic alloys behave in tendency like Ti.

3.3. Characterisation of passive layers

For a more detailed characterisation of the anodic passive layer growth reactions on the eutectic alloys and on their constituent single phases, anodic potentiostatic polarisation experiments at 0.5 V vs. SCE were performed in 0.1 M H_2SO_4 and 0.1 M NaOH solutions for 60 min. The resulting current transients (not shown) do not reveal a purely high-field-controlled passive film growth regime as it is typical for valve metals, like Ti forming TiO_2 [18–20]. The observed characteristics rather indicated the growth of more complex films due to superimposing oxidation reactions of the constituent elements. Additional possible compositional changes of the primary film grown before the anodic potentiostatic polarisation might affect also the current transients.

Due to the ultrafine distribution of the phases in the eutectic alloys, a clear identification of the role of each phase in the passive layer growth is not possible by AES depth profiling. Therefore, AES depth profile analysis was conducted on the passivated surfaces of the constituent single phases of the eutectic alloys.

Fig. 6 shows exemplary AES depth profiles of the surface regions of the single constituent phases of $Ti_{67.79}Fe_{28.36}Sn_{3.85}$ passivated in 0.1 M H_2SO_4 and in 0.1 M NaOH, respectively. Table 1 summarizes the AES results of the samples which were passivated anodically in electrolytes and in air for 7 days. It shows the average concentration of the constituent elements in the oxide film and the sputter time until the oxygen concentration reaches half of its initial value ($O_{1/2}$) during depth profiling, which corresponds to a mean thickness of the oxide layer. A material removal rate during sputtering of a TiO_2 standard of 1.4 nm/min was used to estimate the layer thicknesses being in the range of 1.5–5.5 nm. In all environments the oxide layers formed on the TiFe intermetallic phase ($Ti_{51}Fe_{49}$ and $Ti_{52.5}Fe_{46.8}Sn_{0.7}$) are thinner than those formed on the β-Ti phases ($Ti_{80}Fe_{20}$ and $Ti_{82.3}Fe_{9.2}Sn_{8.5}$). Air-grown oxide layers on the Sn-containing phases are thinner than those on the binary phases. No significant effect of Sn has been observed on anodically grown passive layers in electrolytes. Furthermore, layers grown in NaOH solution are generally thicker than those grown in acidic solution and exhibit a sandwich structure with Fe depletion at the interface to the electrolyte.

Table 1
AES depth profiling of surfaces of the single phase polycrystalline specimens: sputter times until the half-value of oxygen concentration ($O_{1/2}$) (1 min corresponds to 1.4 nm TiO_2) and average concentration of elements in the oxide layers grown in air and potentiostatically for 1 h at 500 mV vs. SCE in 0.1 M H_2SO_4 and 0.1 M NaOH, respectively.

Phase/media	Ti–Fe system			Ti–Fe–Sn system			
	Sputter time ($O_{1/2}$) [min]	Concentration [at.%]		Sputter time ($O_{1/2}$) [min]	Concentration [at.%]		
		Fe	Ti		Fe	Ti	Sn
β-Ti phase/air	2.75	18	22	1.25	10	21	3
TiFe phase/air	1.75	25	15	1	27	15	0
β-Ti phase/NaOH	3.5	14	22	3.75	12	21	1
TiFe phase/NaOH	2.5	22	19	2.75	23	19	0
β-Ti phase/H_2SO_4	2.25	10	22	2	10	22	2
TiFe phase/H_2SO_4	1.5	19	21	1.5	18	22	0

The oxides grown on the β-Ti solid solutions are enriched in Fe compared to the bulk compositions. For the TiFe intermetallic phases, an Fe enrichment was only observed for oxides formed in air. Sn can only be identified in the oxide layers on the β-Ti phases and is detected only in the metallic state. It is almost homogeneously distributed in surface layers formed in H_2SO_4. In contrast, it is only enriched at the interface between metal and oxide for films formed in air and or in NaOH solution.

No significant impact of Sn is found for anodically grown oxide layers regarding thickness and composition. But the thicknesses of air formed oxide layers are much lower for the ternary alloy system.

The lower thickness of the oxides formed on the TiFe intermetallic phases as well as their higher concentration of Fe species can explain the higher reactivity of these phases compared to the β-Ti solid solution as observed in the potentiodynamic polarisation investigations (Fig. 3). The higher reactivity of $Ti_{70.5}Fe_{29.5}$ compared to that of $Ti_{67.79}Fe_{28.36}Sn_{3.85}$ in acidic media cannot be explained by modified passive layer properties. The changes in thickness and composition of the oxide layers grown on the constituent phases due to Sn addition are not significant. Thus, the difference in activity of the eutectic alloys without and with Sn is believed to have its origin in the refined microstructure of $Ti_{67.79}Fe_{28.36}Sn_{3.85}$. This may lead to a laterally more homogeneous passive layer growth yielding a higher protective effect.

3.4. Pitting corrosion

The pitting susceptibility of the eutectic alloys and their constituent single phase polycrystalline specimens was firstly investigated in 0.1 M H_2SO_4 containing 0.1 M KCl. In such chloride-containing solution the anodic behaviour of the constituent phases is quite variable and the values of characteristic corrosion parameters, i.e. corrosion current density, passive current density and passive layer breakdown or pitting potential scatter significantly. Fig. 7 shows examples of anodic polarisation curves. Both eutectic alloys (not shown) and the Sn-containing β-Ti solid solution remain passive in the investigated potential range. Both TiFe intermetallic phases exhibit pitting corrosion at potentials higher than 0.7 V vs. SCE, whereby $Ti_{51}Fe_{49}$ exhibits a higher susceptibility as evident from a more negative breakdown potential. Local breakdown of passivity is observed for the binary β-Ti solid solution only at potentials exceeding 1.2 V vs. SCE, but not for the ternary β-Ti solid solution. This suggests that also $Ti_{67.79}Fe_{28.36}Sn_{3.85}$ may be less susceptible to pitting corrosion than $Ti_{70.5}Fe_{29.5}$. However, both eutectic alloys show no breakdown of passivity in 0.1 M H_2SO_4 + 0.1 M KCl. Therefore, it can again be concluded that the microstructures of the alloys are crucial for the protective character of the oxide layers.

The eutectic alloys were further investigated in acidic solutions with higher chloride concentrations. Potentiodynamic polarisation tests were performed in 0.1 M H_2SO_4 containing 0.5 M and 1 M KCl and in 0.5 M, 1 M and 3 M HCl. Typical curves are shown in Fig. 8. While $Ti_{70.5}Fe_{29.5}$ remains in a stable passive state even up to 3 M HCl, $Ti_{67.79}Fe_{28.36}Sn_{3.85}$ exhibits pitting corrosion in the solutions containing 1 M chloride ions, i.e. 0.1 M H_2SO_4 + 1 M KCl and in 1 M HCl. Repeated measurements in these solutions reveal a remarkable scattering of the critical pitting potential, which varies from 0.2 V vs. SCE to stable passivity in the investigated potential range, i.e. up to 2 V vs. SCE. In 3 M HCl $Ti_{67.79}Fe_{28.36}Sn_{3.85}$ dissolves actively already at the free corrosion potential. Therefore, $Ti_{67.79}Fe_{28.36}Sn_{3.85}$ is more susceptible to pitting corrosion. Such enhanced susceptibility

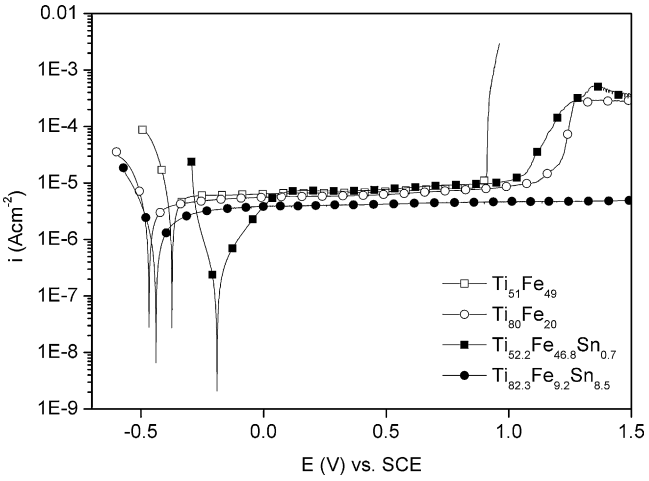

Fig. 7. Current density–potential curves of the constituent phases of the eutectic alloys recorded in 0.1 M H_2SO_4 + 0.1 M KCl (scan rate of 0.5 mV/s).

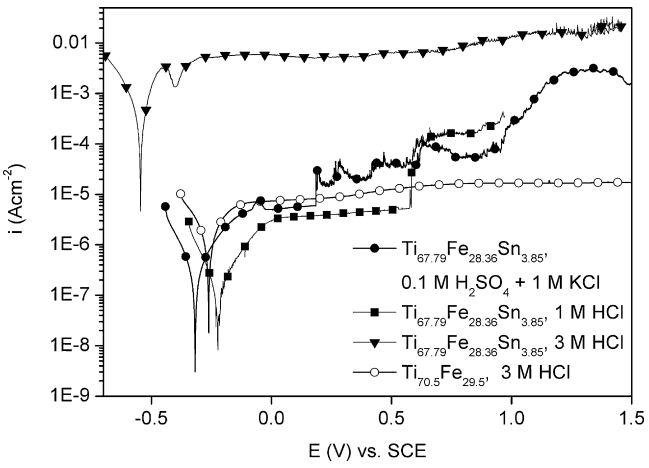

Fig. 8. Current density–potential curves of the eutectic alloys recorded in acidic media with varying concentrations of chloride ions (scan rate of 0.5 mV/s).

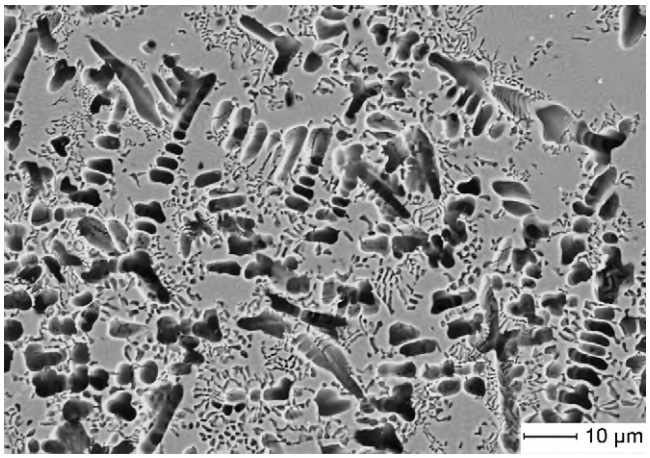

Fig. 9. SEM image of $Ti_{67.79}Fe_{28.36}Sn_{3.85}$ showing the surface morphology after potentiodynamic polarisation in 0.1 M H_2SO_4 + 1 M KCl.

is originated due to the microstructure because the Sn-containing polycrystalline single phases exhibited a lower susceptibility. Fig. 9 shows the surface of a $Ti_{67.79}Fe_{28.36}Sn_{3.85}$ sample with characteristic chloride-induced corrosion damage morphology. The pitting started preferentially at the border regions of the eutectic cells, where large fractions of the more reactive $Ti_{51}Fe_{49}$ are exposed to the electrolyte. Once a pit is initiated the β-Ti phase can dissolve as well. However, it is visible that single lamellae of the TiFe phase also dissolve. Thus, the larger fraction of the TiFe intermetallic phase and its larger cross-sectional areas in $Ti_{67.79}Fe_{28.36}Sn_{3.85}$ at the borders of the eutectic cells compared to the volume fraction and surface area of the TiFe phase in $Ti_{70.5}Fe_{29.5}$ cannot be the only reason for the enhanced pitting susceptibility. The lattice parameter of the β-Ti phase is enhanced from 0.3165 nm in Ti(Fe) to 0.3263 nm in Ti(Fe,Sn) while it is almost unaffected by the addition of Sn in the TiFe phase (0.2995 nm in TiFe and 0.2988 in TiFe(Sn), respectively) [13]. This leads to an increase of the lattice parameter difference between the eutectic alloys constituent phases from 0.017 nm in $Ti_{70.5}Fe_{29.5}$ to 0.028 nm in $Ti_{67.79}Fe_{28.36}Sn_{3.85}$ what might alter the structure of the passive layer at the interface of the individual lamella and can induce local stress into the layer. The newly identified TiSn phase is obviously not an initiation point for pitting.

4. Summary

Both $Ti_{67.79}Fe_{28.36}Sn_{3.85}$ and $Ti_{70.5}Fe_{29.5}$ eutectic alloys exhibit low corrosion rates in aqueous media from pH 1 to 13 due to the spontaneous passivity. The anodic polarisation behaviour can be explained by the known behaviour of the elements Ti and Fe. Compared to the β-Ti solid solutions, the TiFe intermetallic phases show an enhanced reactivity in acidic media due to the formation of thinner passive layers with high Fe content. $Ti_{67.79}Fe_{28.36}Sn_{3.85}$ is more stable than $Ti_{70.5}Fe_{29.5}$ due to the finer distribution of the constituent ultrafine phases resulting a more homogeneous passive layer with improved protective properties. In general, the TiFe(Sn) intermetallic phases are more susceptible to pitting corrosion than the β-Ti(Fe,Sn) solid solutions. In acidic media $Ti_{67.79}Fe_{28.36}Sn_{3.85}$ exhibits a higher pitting susceptibility than $Ti_{70.5}Fe_{29.5}$. The enhanced pitting susceptibility of $Ti_{67.79}Fe_{28.36}Sn_{3.85}$ compared to than that of $Ti_{70.5}Fe_{29.5}$ is due to the larger lattice misfit between the constituent phases.

Both eutectic alloys are very stable and applicable in a wide range of pH values, even in strongly acidic environments. As long as chloride ions are present only in small concentrations the ternary eutectic alloy is favourable due to its improved mechanical properties and high corrosion resistance. In strongly acidic media containing high concentrations of chloride ions the binary eutectic alloy is favourable due to its higher stability against pitting corrosion.

Acknowledgements

The authors thank M. Frey and G. Lindenkreuz for alloy preparation.

J. Das acknowledges the Defense Research Development Organisation, New Delhi, India for the financial support.

References

[1] E.O. Hall, Proc. Phys. Soc. Lond. B 64 (1951) 747–753.
[2] N.J. Petch, J. Iron Steel Inst. 174 (1953) 25–28.
[3] Q. We, D. Jia, K.T. Ramesh, E. Ma, Appl. Phys. Lett. 81 (2002) 1240–1242.
[4] D.V. Louzguine, H. Kato, A. Inoue, J. Alloys Compd. 384 (2004) L1–L3.
[5] C.C. Hays, C.P. Kim, W.L. Johnson, Phys. Rev. Lett. 84 (2000) 2901–2904.
[6] G. He, J. Eckert, W. Löser, L. Schultz, Nat. Mater. 2 (2003) 33–37.
[7] Y. Wang, M. Chen, F. Zhou, E. Ma, Nature 419 (2002) 912–915.
[8] J. Das, K.B. Kim, F. Baier, W. Löser, A. Gebert, J. Eckert, J. Alloys Compd. 434–435 (2007) 28–31.
[9] S. Mato, G. Alcala, T.G. Woodcock, A. Gebert, J. Eckert, L. Schultz, Electrochim. Acta 50 (2005) 2461–2467.
[10] W. Zeiger, M. Schneider, D. Scharnweber, H. Worch, Nanostruct. Mater. 6 (1995) 1013–1016.
[11] H.Y. Tong, F.G. Shi, Scripta Metall. Mater. 32 (1995) 511–516.
[12] A. John, W. Zeiger, D. Scharnweber, H. Worch, S. Oswald, Fresen. J. Anal. Chem. 365 (1999) 136–141.
[13] J. Das, K.B. Kim, F. Baier, W. Löser, J. Eckert, Appl. Phys. Lett. 87 (2005), 161907-1–161907-3.
[14] J. Das, K.B. Kim, W. Xu, W. Löser, J. Eckert, Mater. Sci. Eng. A 449 (2007) 737–740.
[15] W.W. Scott, Binary Alloy Phase Diagrams, vol. 2, second ed., ASM International, 1990, pp. 3405–3407.
[16] J. Das, F. Ettinghausen, J. Eckert, Scripta Mater. 58 (2008) 631–634.
[17] T. Hurlen, W. Wilhelmsen, Electrochim. Acta 31 (1986) 1139–1146.
[18] T.R. Beck, J. Electrochem. Soc. 129 (1982) 2500–2501.
[19] N. Cabrera, N.F. Mott, Rep. Prog. Phys. 12 (1948) 163–184.
[20] G.T. Burstein, A.J. Davenport, J. Electrochem. Soc. 136 (1989) 936–941.